

Large Hadron Collider Project

LHC Project Report 158

**Simulations for the Beam-Induced Electron Cloud in the LHC beam screen with
Magnetic Field and Image Charges**

Oliver S. Brüning

Abstract

The paper presents new simulation results for the beam-induced electron cloud in the LHC beam screen. All simulations are carried out using an improved two-dimensional module for the space charge and image charge calculations. The work gives a systematic investigation of the dependence of the heat load on several parameters and gives a brief discussion of possible cures. The work investigates only the regions with strong vertical magnetic field.

Administrative Secretariat
LHC Division
CERN
CH-1211 Geneva 23
Switzerland

Geneva, 7 November 1997

1 Introduction

The synchrotron radiation in the LHC creates a continuous flow of photo-electrons. These electrons are accelerated by the electric field of the bunch and hit the vacuum chamber on the opposite side of the beam pipe where they create secondary electrons which are again accelerated by the next bunch. In the field free regions, the accelerated electrons move radially towards the beam center and the particle dynamics is a one-dimensional problem. In the strong dipole field, the electron motion is effectively confined to a motion along the vertical field lines and the energy gain of an electron during the bunch passage does not only depend on its radial distance from the beam but also on its horizontal position inside the beam pipe. Consequently, the average energy gain of the electrons in the field-free regions during a bunch passage is larger than in the regions with strong dipole field. On the other hand, it is also much easier to influence the electron motion with external fields in the field free regions than in the regions with strong dipole fields. For example, one can eliminate the electrons in the field free region with a small solenoid field of only 10 to 50 Gauss [1]. Inside a strong dipole field such a small perturbation has no visible effect on the electron motion and it is more difficult to cope with the electrons in these regions. The following study concentrates only on the heat load in regions with a strong vertical dipole field, which covers approximately 65 % of the machine circumference.

Depending on the photo yield for the production of photo-electrons, the secondary emission yield and the reflectivity, the heat load can vary from 0.1 W/m to more than 15 Watt/meter inside the dipole magnets. The current budget of the cryogenic system is based on an electron cloud-induced heat load of 0.2 W/m and can not tolerate a heat load of more than 0.5 W/m . Thus, the design of the beam screen must assure a heat load which is smaller than this amount.

Because the heat load depends on the reflectivity, photo and secondary yield of the beam screen, it is mandatory to get accurate estimates for these parameters before any feed-back can be given to the design of the beam screen. Currently there are two different programs which are used for estimating the heat load in the LHC beam screen due to photo-electrons: one code from M. Furman which was developed at LBL [2] and one based on a program by F. Zimmermann [3] which was further developed at CERN in order to study the heat load in the beam screen. In a previous note, we presented first numerical simulations for the beam-induced electron cloud in the LHC beam screen using the second program [4]. Since then, the simulation program has been modified to incorporate the effect of image charges on the vacuum chamber induced by the passing beam and the electrons in the chamber. Furthermore, the modules for the space charge calculation and the generation of secondary electrons have been replaced by new routines which better model the three-dimensional dynamics of the electrons in the vacuum chamber. New measurements of the photon yield and reflectivity of different surface materials at CERN [5] are taken into account and heat load estimates are given for the new parameters.

The availability of two independent simulation programs for the heat load generation in the beam screen has proven to be extremely useful. A continuous comparison of the results generated by the two programs indicated several weak points in the algorithms and finally led to an improvement of both programs. While the results initially disagreed by more than a factor of two, they now differ by less than 20%, giving us good confidence in the results.

The following work summarises the simulation results obtained at CERN and looks at possible cures for the heat load in the beam screen. The paper is structured as follows: First, we will briefly summarise the main assumptions in the simulation program and discuss the main parameters relevant for the heat load. Next, we introduce the notion of a critical secondary

emission yield which divides the parameter space in two qualitatively different subspaces. The fourth section presents results for the heat load in the LHC beam screen for different sets of parameters. The fifth section discusses potential cures and improvements for the heat load and the results are summarised in a final section.

2 Simulation Model and Beam Parameters

In all simulations we assume a Gaussian longitudinal bunch distribution and cut the bunch into 50 slices. Electrons close to the beam will oscillate in the beam potential and cutting the bunch into slices allows a proper modelling of the electron motion during the bunch passage. With less than 50 slices per bunch the simulation can not properly reproduce these oscillations, leading to an overestimate of the energy gain of the electrons during the bunch passage. A larger number of slices does not further improve the simulation results.

During the bunch passages we generate new photo-electrons. The total number of photons emitted by a charged particle per radian is given by [6]

$$N_\gamma = \frac{5}{2\sqrt{3}}\alpha\gamma, \quad (1)$$

where α is the fine-structure constant and γ the Lorenz factor. For protons at 7 TeV the critical energy of these photo-electrons is

$$E_{crit.} = \frac{3\hbar c}{2\rho} \cdot \gamma^3 \quad (2)$$

$$= 44 \text{ eV} \quad (3)$$

and the total number of photo-electrons with energies larger than 4 eV (the work function of Cu) is approximately

$$N_{bunch} \cdot Y \cdot 0.17 \quad (4)$$

photons per bunch where N_{bunch} is the number of protons per bunch and Y the photo-electron yield. For all calculations we assumed a Gaussian energy distribution of the photo-electrons around 7 eV and a width of $\sigma_{pe} = 5 \text{ eV}$. However, the final energy distribution of the photo-electrons is mainly determined by the energy gain during the bunch passage and the initial distribution has only a small influence on the final results.

In the simulation program the electrons are modelled by macro-particles which initially carry the same charge. In all simulations we generate between 1000 and 5000 macro particles per bunch. The number of macro-particles generated per beam slice is proportional to the number of protons inside the slice. For each slice we first generate the new photo-electrons and then evaluate the force of the beam slice on the electrons. Thus, newly generated photo-electrons experience only a fraction of the full beam kick, depending on whether they are generated near the head or the end of the bunch. On the other hand, secondary electrons from a previous bunch will always experience the full beam kick. For a non-circular beam pipe the image charges of the beam on the vacuum chamber are included in the beam kick on the electrons.

The gap between two bunches is again divided into 50 steps, allowing a proper modelling of the particle motion under the influence of space charge and detecting the electron losses at the proper positions. However, the recalculation of the space charge field is very time consuming and, unless otherwise stated, the space charge field is calculated only once right after the bunch

passage. For the space charge field calculation we assume a four-fold symmetry of the electron cloud and map all electrons into one quadrant of the transverse plane. In a second step, we calculate the horizontal and vertical electric field components of the electron cloud on a 25 times 25 mesh and store the results on a two dimensional matrix for tracking. An additional option allows the generation of image charges which lead to a equipotential surface at the vacuum chamber.

Once an electron reaches the boundary of the vacuum chamber the program calculates the secondary emission yield of the incident electron as a function of its energy and incident angle with respect to the surface normal. The charge of the emitted macro particle is given by the product of the initial charge and the secondary emission yield $\delta(E, \theta)$. For the secondary emission yield we assume [7]

$$\delta(E, \theta) = \delta_{max} \cdot 1.11 \cdot \left(\frac{E}{E_{max}}\right)^{-0.35} \cdot \left(1 - \exp\left[-2.3 \cdot \left(\frac{E}{E_{max}}\right)^{1.35}\right]\right) / \max(\cos \theta, 0.2), \quad (5)$$

where θ is the angle of the incident electron with respect to the surface normal, E the electrons energy, E_{max} the energy for which the secondary emission yield has a maximum and δ_{max} the maximum secondary emission yield for normal incidence of the electron. In the following we assume $E_{max} = 400 \text{ eV}$ for all simulations and limit the value of $\cos \theta$ to values larger than 0.2. Fig. 1 shows the secondary emission coefficient for normal incident and $\delta_{max} = 1.4$. The θ dependence of the secondary yield implies an influence of the shape of the vacuum chamber on the electron cloud density. In the following, we look at two different geometries: an elliptical vacuum chamber and an LHC-type chamber with a flat section on top and bottom. Both geometries are shown in Fig. 2 and the corresponding dimensions are given in Table 1. However, the calculation of the image charges is based on an elliptical boundary in both cases.

	hor. diameter d_h	vert. diameter d_v
LHC-type chamber	44 mm	36 mm
Elliptical chamber	44 mm	36 mm

Table 1: *Horizontal and vertical diameters of the vacuum chambers.*

The energy distribution of the emitted macro particle is determined by a Monte Carlo algorithm which, in principle, can generate an arbitrary distribution. However, at this point, the initial energy distribution of the secondary electrons in the LHC beam screen is still an unknown parameter and we studied the dependence of the heat load on this parameter by assuming a half Gaussian distribution around 0 eV with the distribution width σ_{se} being a free parameter. The distribution is cut at $5\sigma_{se}$. Currently there is an ongoing effort at CERN to measure the energy distribution of the secondary electrons for different surfaces. First results indicate that most secondary electrons are emitted at low energies (between 0 eV and 2 eV) [5], but an accurate measurement of the distribution function is not yet available. In the following we will consider different Gaussian distributions with σ_{se} between 0 eV and 20 eV. Essentially, the value of σ_{se} determines how many secondary electrons remain inside the vacuum chamber before the next bunch arrives. Because of their small initial energy, all secondary electrons which reach the vacuum chamber before the next bunch arrives are lost and do not contribute to the heat load in the beam screen.

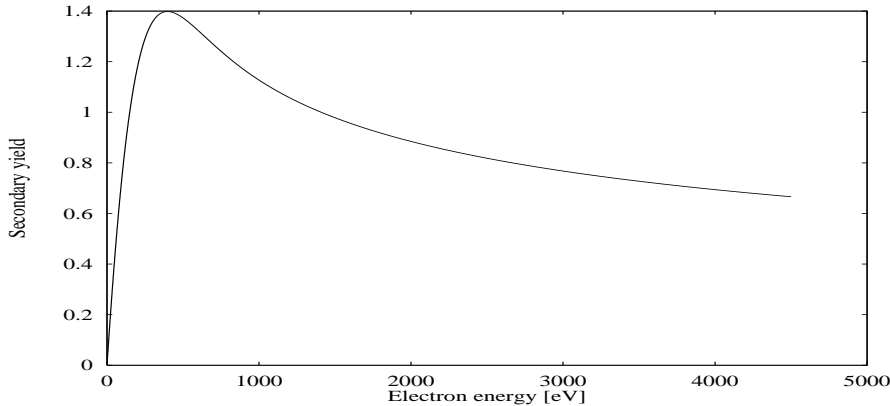


Figure 1: *The secondary yield for normal incident as a function of the electron energy for $\delta_{max} = 1.4$.*

If the energy of the incident particle is smaller than the energy of the newly generated secondary electron, the incident particle is absorbed without generating a new electron. This procedure affects only low energetic electrons with energies smaller than $5\sigma_{se}$ and ensures energy conservation. In order to account for the fact that the secondary electrons will tend to exit the vacuum chamber parallel to the surface normal we distribute the kinetic energy of the secondary electrons randomly on the three degrees of freedom such that the motion parallel to the surface normal carries on average half of the total kinetic energy. The other half of the kinetic energy is uniformly distributed over the other two degrees of freedom.

In regions with a strong dipole field the heat load depends not only on the photon and secondary emission yield, but also on the surface reflectivity. In case of a high reflectivity the photo electrons are approximately uniformly distributed over the surface of the beam screen. For a small reflectivity, they are mainly generated within the horizontal plane of the beam screen. In the presence of a strong vertical magnetic field these electrons can not reach the center of the beam pipe and will only experience a small energy gain during the bunch passage (we will come back to this point in Section 4.4). In the case of a non-negligible reflectivity, the measured photo yield can be too small if the photo-electrons produced at higher reflection levels are not detected [8]. In order to correct for this effect, we follow the procedure in [9] and define the effective quantum yield by

$$Y = y \cdot \frac{1}{1 - R}, \quad (6)$$

where y is the measured photo yield and R the reflectivity. The latest reflectivity measurements at CERN using synchrotron light from the EPA ring showed an effective quantum yield of the order of $Y \approx 0.15$ [5] for an electro-plated vacuum chamber, where the photo yield is defined as the ratio of measured photo-electrons and the number of photons with energies higher than the work-function of the surface (4 eV). The reflectivity was approximately $R \approx 5.0\%$ [5]. Old measurements on a roll-bonded copper surface gave an effective quantum yield of $Y \approx 0.21$ and a reflectivity $R \approx 82.0\%$ [5]. Table 2 summarises the relevant beam parameters of the LHC.

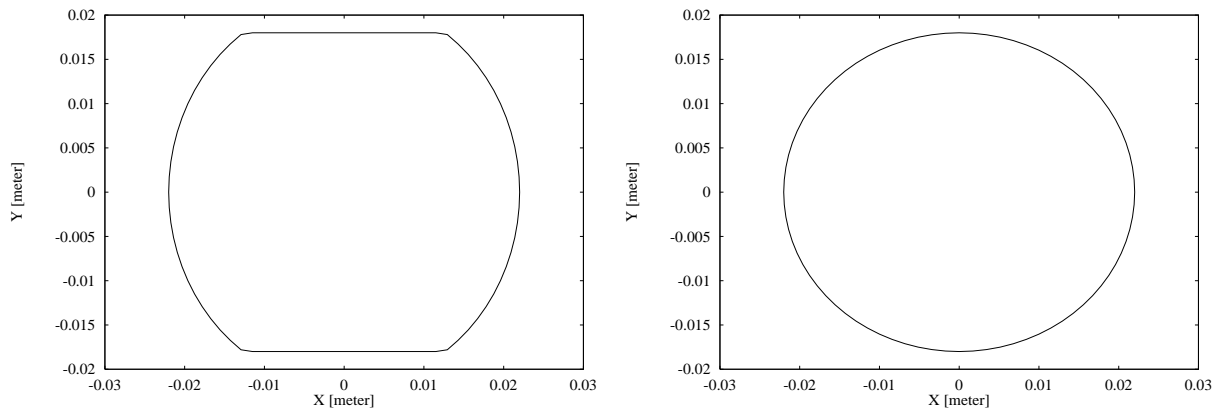


Figure 2: *Left: The geometry of the LHC-type vacuum chamber. Right: An elliptical vacuum chamber with comparable dimensions.*

E [eV]	N_b	N_p	σ_x [m]	σ_y [m]	σ_z [m]	b_s [ns]	b_l [m]	B [T]	E_γ [eV]
7000	2835	$1.05 \cdot 10^{11}$	0.303	0.303	0.075	25	14.2	8.4	44.1

Table 2: *Beam parameters for the LHC. E is the beam energy, N_b is the number of bunches in the storage ring, N_p the number of particles per bunch, σ_x, σ_y and σ_z are the horizontal, vertical and longitudinal bunch sizes, b_s is the bunch distance in seconds, b_l the bending magnet length, B the bending field at top energy and E_γ the critical energy of the synchrotron light photons.*

3 Maximum secondary yield without exponential growth

In this section we look for the maximum secondary yield coefficient δ_{max} for which we do not observe an exponential growth of the electron cloud. If the secondary emission coefficient of the vacuum chamber is much smaller than this critical value, the heat loss will be approximately proportional to the number of synchrotron light photons and the photon yield. If it is larger than this value, the heat loss will be determined by the value of δ_{max} and even a single electron, e.g. from residual gas ionisation, is sufficient to trigger the build up of an electron cloud. Clearly, when designing a beam screen for the LHC vacuum chamber it is necessary to achieve a secondary emission coefficient which is smaller than the critical yield value and it becomes important to understand how the critical value depends on the beam parameters and the vacuum chamber geometry.

As a bunch passes through a bending magnet, its synchrotron radiation generates photo-electrons at the wall of the beam screen. The photo electrons are accelerated by the beam and hit again the beam screen on the opposite side of the vacuum chamber where they create low energy secondary electrons. In the presence of a dipole magnetic field, the electrons move effectively only in the vertical direction parallel to the magnetic field lines. Fig. 3 shows the corresponding energy and velocity distributions of the accelerated primary photo-electrons in the presence of a vertical magnetic field and for the beam parameters given in Table 2. The average velocity of the accelerated photo-electrons is approximately $0.013 \cdot c$ (the average energy is approximately 80 eV). The average energy of the accelerated secondary electrons hitting the

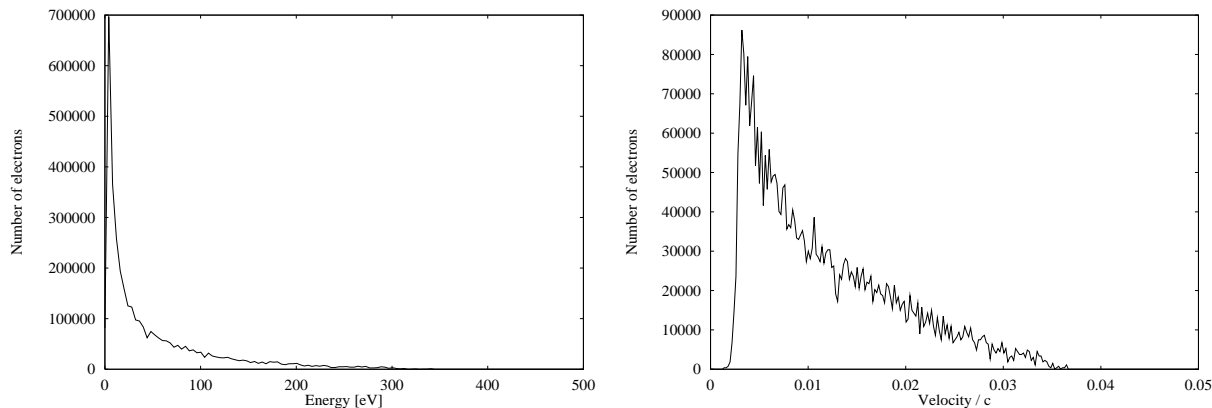


Figure 3: *The LHC-type vacuum chamber with a vertical magnetic field of 8.4 T. Single bunch passage.*

Left: The energy distribution for the photo-electrons of a Gaussian bunch.

Right: The corresponding velocity distribution.

vacuum chamber varies between 300 eV and 400 eV [4]. The left-hand side of Fig. 4 shows the energy distribution of the electrons for an elliptical vacuum chamber with a maximum secondary emission coefficient of $\delta_{max} = 1.4$, an effective quantum yield of $Y = 0.4$ and a Gaussian initial energy distribution for the secondary electrons with $\sigma_{se} = 10$ eV. The average electron energy is $\langle E_e \rangle \approx 380$ eV.

The maximum vertical distance between two opposite sides of the beam screen is 36 mm. Thus, it takes the photo-electrons on average 9 ns to traverse the vacuum chamber compared with a bunch spacing of approximately 25 ns in the LHC. In order to be accelerated by the next bunch the low energetic secondary electrons have to survive on average 16 ns. If they are lost before the next bunch arrives, they will not contribute to the heat load on the beam screen. In our simulations we assume a half-Gaussian energy distribution for the secondary electrons with a sigma of $\sigma_{se} = 10$ eV and cut at 5σ . The right-hand side of Fig. 4 shows the initial energy distribution of the secondary-electrons. Assuming for the moment that the energy of the secondary electrons is equally distributed over the three degrees of freedom, all secondary electrons with an energy larger then $E_{sec} \approx 10$ eV will be lost before the next bunch arrives. For the energy distribution on the right-hand side of Fig. 4 this implies that more then half of all secondary electrons are lost. Thus, in order to built up electrons in the vacuum chamber, the average secondary yield must be large enough to compensate for the lost secondary electrons. This interpretation implies a strong influence of the energy distribution of the secondary electrons on the critical value of δ_{max} . Using the same line of argumentation one can show that the bunch spacing and the diameter of the vacuum chamber have a similarly strong effect on the critical secondary yield ($SEY_{crit.}$).

In order to find the critical secondary yield, we neglect the space charge effects and generate photo-electrons only for the first bunch. Looking at the evolution of the number of electrons per unit length over 60 bunch passages, the electron density will decrease if the secondary emission yield is smaller then the critical value. If the secondary emission yield is

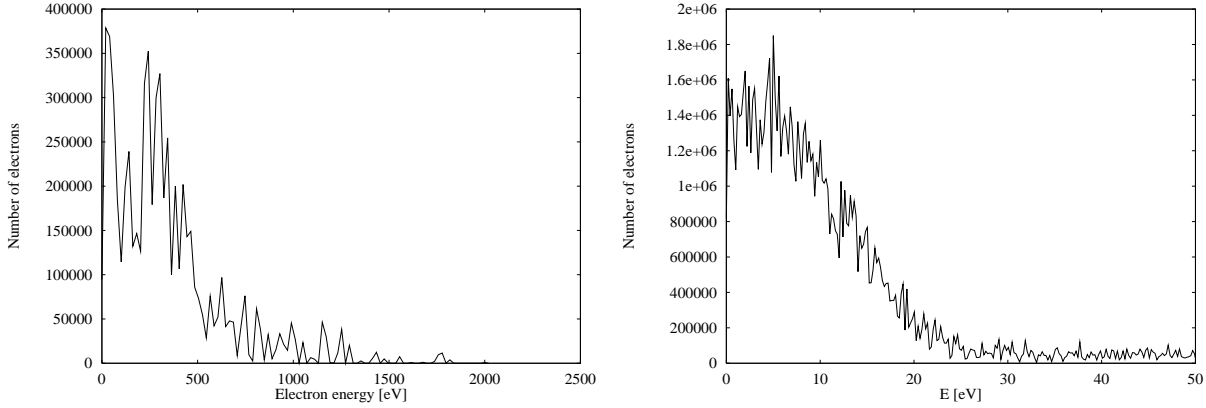


Figure 4: *Left: The energy distribution of the electrons for an elliptical vacuum chamber with a magnetic field of 8.4 T, a maximum secondary yield $\delta_{max} = 1.4$, an effective quantum yield of $Y = 0.4$ and a uniform azimuthal distribution of the photoelectrons (space charge forces are included).*

Right: The initial energy distribution of the secondary electrons.

larger, the electron density will grow exponentially. Fig. 5 shows the evolution of the number of electrons per unit length for the LHC-type vacuum chamber. The left-hand side shows the evolution of the number of electrons per unit length for $\delta_{max} < SEY_{crit.}$ and the right-hand side for $\delta_{max} > SEY_{crit.}$.

For the nominal LHC beam parameters in Table 2 and a Gaussian distribution with $\sigma_{se} = 10$ eV for the initial energy of the secondary electrons one obtains a critical secondary emission coefficient of

$$SEY_{crit.} = 1.4. \quad (7)$$

For comparison, Table 3 shows the value of δ_{max} for different surfaces [12]. Except for TiN,

Material	TiN	Ti	Stainless Steel	Cu	Al
δ_{max}	1.066	1.9	2.0	2.1	3.5

Table 3: *Secondary emission coefficient δ_{max} for different materials. (The δ_{max} of TiN is only reached after a massive bombardment with electrons.)*

the values for δ_{max} vary between 1.9 for Ti and 3.5 for Al and the critical secondary emission coefficient for the nominal LHC beam parameters is smaller than δ_{max} for most surface materials available for the LHC beam screen. (The δ_{max} of TiN is only 1.066 but this value is only reached after a massive electron bombardment.)

The left-hand side of Fig. 6 shows the $SEY_{crit.}$ as a function of the width of the initial energy distribution for the secondary electrons. The other parameters are as in Table 2. As we mentioned earlier, it is necessary to have a secondary emission coefficient which is smaller than the critical value $SEY_{crit.}$. However, the left-hand side of Fig. 6 shows that $SEY_{crit.}$ approaches unity for decreasing σ_{se} . Thus, for small values of σ_{se} it is impossible to have a secondary

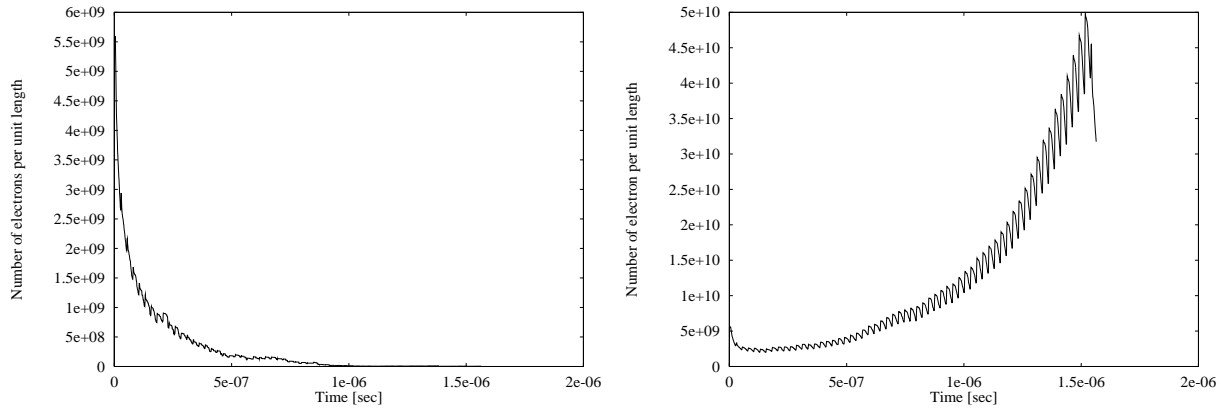


Figure 5: *LHC-type vacuum chamber with a magnetic field of 8.4 T. photo-electrons are only generated for the first bunch:*

Left: The evolution of the number of electrons per unit length in the vacuum chamber with $\delta_{max} < SEY_{crit}$.

Right: The evolution of the number of electrons per unit length in the vacuum chamber with $\delta_{max} > SEY_{crit}$.

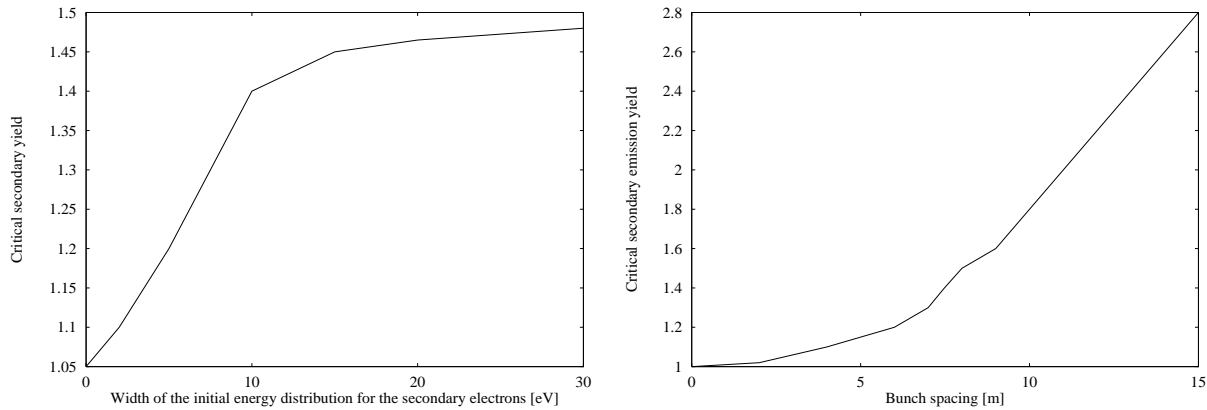


Figure 6: *Left: The critical secondary yield parameter versus the width of the initial energy distribution of the secondary electrons (space charge fields neglected).*

Right: The critical secondary yield parameter versus the bunch separation for a Gaussian initial energy distribution of the secondary electrons with $\sigma_E = 10$ eV.

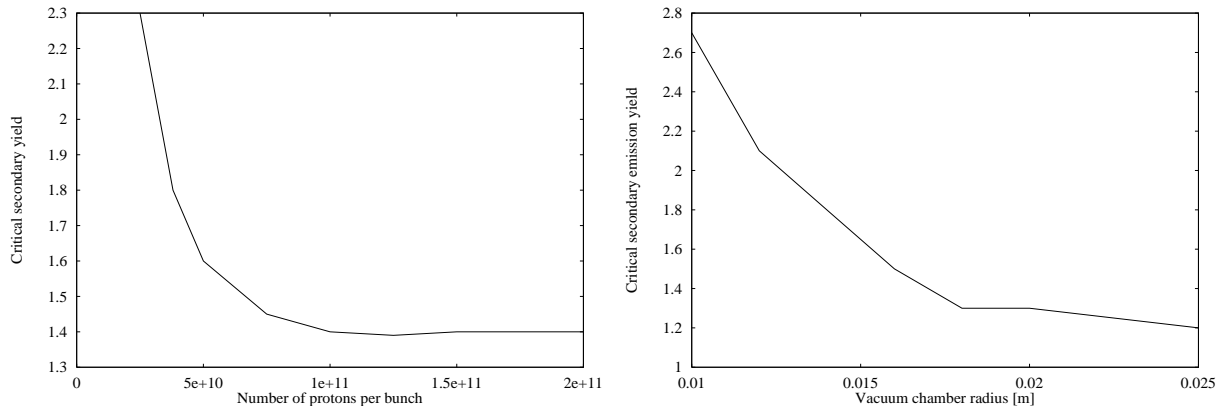


Figure 7:

Left: The critical secondary yield parameter versus the bunch intensity.

Right: The critical secondary yield parameter versus the vacuum chamber radius (assuming a round chamber).

In both cases we assumed a Gaussian energy distribution with $\sigma_E = 10$ eV.

emission yield which is smaller than $SEY_{crit.}$ (see Table 3) and any number of initial photoelectrons can trigger the build-up of an electron cloud with a large heat load. Preliminary measurement shows that the initial energy distribution of the secondary electrons is indeed very narrow with values of σ_{se} close to 1 eV or 2 eV [5], indicating a potential problem for the LHC. However, it turns out that secondary electrons with such small values for σ_{se} are strongly affected by their own space charge field. The space charge field repels a large fraction of the electrons back into the beam pipe and thus, reduces the heat load in the beam screen. We will come back to this point later in Section 4.6.

The right-hand side of Fig. 6 shows the $SEY_{crit.}$ as a function of the bunch spacing with $\sigma_{se} = 10$ eV. All other parameters are as in (2). In this case, $SEY_{crit.}$ increases with increasing bunch spacing. For example, doubling the bunch spacing in the LHC will increase $SEY_{crit.}$ from $SEY_{crit.} = 1.4$ to $SEY_{crit.} = 2.8$, which is larger than the secondary emission coefficient of most materials in Table 3. Thus, a larger bunch spacing will clearly reduce the heat load in the beam screen. On the other-hand, increasing the bunch spacing in the LHC by a factor 2 will also reduce the total number of bunches in the machine and the luminosity by the same factor. The experimental insertion in the LHC are another example where the effect of the bunch spacing on the heat load might be important. In these regions, both beams share the same beam pipe and the effective bunch spacing seen by the electron cloud is only half of the nominal value. In this case, one obtains $SEY_{crit.} \approx 1.1$, indicating a potentially high heat load in these regions.

The left-hand side of Fig. 7 shows the $SEY_{crit.}$ as a function of the bunch intensity. While $SEY_{crit.}$ decreases with increasing bunch intensity for $N_b < 10^{11}$, it remains approximately constant for bunch intensities larger than $N_b = 10^{11}$. The reason for this is that for the nominal beam intensity the average energy gain per bunch passage ($\langle E \rangle \approx 300$ eV) is already close to the maximum of the secondary yield curve given in Fig. 1. Increasing the bunch intensity will increase the average energy gain per bunch passage but the secondary yield curve does

not change much for energies larger than 400 eV. The secondary yield varies approximately linear with energy only for energies smaller than 200 eV and lowering the bunch intensity below $N_b = 1.05 \cdot 10^{11}$ increases the value of $SEY_{crit.}$. Thus, in order to obtain large values for $SEY_{crit.}$ it would be beneficial to have a larger bunch spacing and to compensate the corresponding reduction in luminosity by a higher bunch current. For example, doubling the bunch spacing and increasing the bunch current by a factor $\sqrt{2}$ gives $SEY_{crit.} > 2.5$ while keeping the luminosity constant. This value is still larger than typical values of the secondary emission coefficient δ_{max} for copper surfaces [12]. Unfortunately, such a scenario still reduces the final luminosity of an 'ultimate' beam in the LHC with a bunch current of $N_b = 1.6 \cdot 10^{11}$ and it is preferable to keep a nominal bunch spacing of $b_s = 25$ ns. However, it is still desirable to have this scenario at least as a fall-back option for the LHC operation in case one encounters higher losses than foreseen.

The right-hand side of Fig. 7 shows the $SEY_{crit.}$ as a function of the vacuum chamber radius (assuming a round chamber). We assume again $\sigma_{se} = 10$ eV and all other parameters are as in Table 2. In this case $SEY_{crit.}$ decreases with an increasing beam pipe diameter implying that the heat load due to the electron cloud might be particularly large for sections in the LHC with large pipe radius. For example, the maximum radius in the experimental insertions is larger than 3 cm implying that $SEY_{crit.}$ will be smaller than 1.2.

When we estimated $SEY_{crit.}$ as a function of the initial energy distribution of the secondary electrons (σ_{se}), we neglected the effect of space charge (with space charge, we will never observe an exponential increase of the electron density) and saw that $SEY_{crit.}$ decreases with σ_{se} . However, the total number of electrons which actually remain in the beam pipe until the next bunch arrives can be significantly reduced by space charge forces for small values of σ_{se} . We will discuss this point in more detail in the Section 4.6.

4 Heat load in the LHC Beam Screen

In this section we look at different cases where δ_{max} is smaller/larger than $SEY_{crit.}$ and estimate the heat load in the beam screen as a function of the photon yield Y . Each case is presented in a separate sub-section.

4.1 Nominal beam parameters, high reflectivity and $\delta_{max} = 0$

Neglecting the secondary yield, the heat load in the beam screen is entirely determined by the energy of the photo-electrons. For the nominal LHC parameters, the average kinetic energy of the photo-electrons after the bunch passage is

$$\langle E_{pe} \rangle \approx 80 \text{ eV}. \quad (8)$$

Assuming a photo yield of $Y = 0.2$, and the nominal LHC bunch population ($N_p = 1.05 \cdot 10^{11}$) one expects approximately $3.5 \cdot 10^9$ photo-electrons per bending magnet and bunch (see Equation (4)). The average heat load generated by the photo-electrons is given by

$$W_{pe} = \frac{N_{bunch} \cdot Y \cdot 0.17 \cdot \langle E_{pe} \rangle}{b_s \cdot b_l}. \quad (9)$$

Inserting (8) into (9) one obtains

$$W_{pe}(Y = 0.2) = 0.128 \text{ W/m}. \quad (10)$$

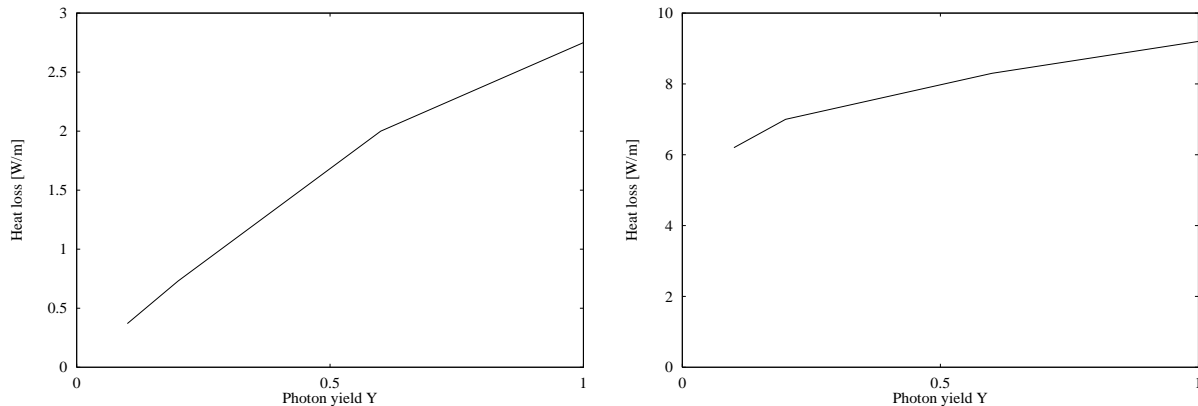


Figure 8: *The heat load in an elliptical chamber for a Gaussian initial energy distribution of the secondary electrons with $\sigma_{se} = 10$ eV.*
Left: $\delta_{max} = 1.066$. Right: $\delta_{max} = 1.8$.

The value in (10) represents the minimum heat load without any contribution of secondary electrons. It should be emphasised that the maximum heat load tolerable for the vacuum system is less than a factor two larger than this minimum contribution and that a photon yield larger than $Y = 0.3$ exceeds already the maximum tolerable value of $W = 0.2$ W/m.

4.2 Nominal beam parameters and high reflectivity

Fig. 8 shows the heat loss for an elliptical vacuum chamber and for nominal beam parameters (see Table 2). Fig. 9 shows similar data for the LHC type chamber. The left-hand side of Fig. 8 shows the heat load for a secondary emission yield of $\delta_{max} = 1.066$ which is smaller than the critical yield SEY_{crit} for the nominal LHC parameters and a Gaussian initial energy distribution of the secondary electrons with $\sigma_{se} = 10$ eV. The right-hand side shows the heat load for a secondary emission yield of $\delta_{max} = 1.8$ which is larger than the critical yield SEY_{crit} for the nominal LHC parameters. Fig. 9 shows similar results for the LHC-type vacuum chamber. The top curves corresponds to $\sigma_{se} = 10$ eV and the lower curves to $\sigma_{se} = 20$ eV.

For a secondary emission yield smaller than SEY_{crit} the heat load in the elliptical chamber is slightly smaller than the heat load in the LHC-type chamber. For a secondary emission yield larger than SEY_{crit} the situation is reversed. However, in both cases the difference is less than 10%. The difference between the two geometries is only relevant for a secondary emission yield close to SEY_{crit} [4].

Assuming a photon yield of $Y = 0.2$ we obtain a heat loss of 0.65 W/m for a secondary emission coefficient of $\delta_{max} = 1.066$, which is already larger than the maximum value tolerable by the cryogenic system. For a secondary emission yield of $\delta_{max} = 1.8$ which is larger than SEY_{crit} one obtains a heat load of more than 7 W/m. While the first value is at least close to the limit tolerable by the vacuum system the second value is clearly too large and can not be tolerated.

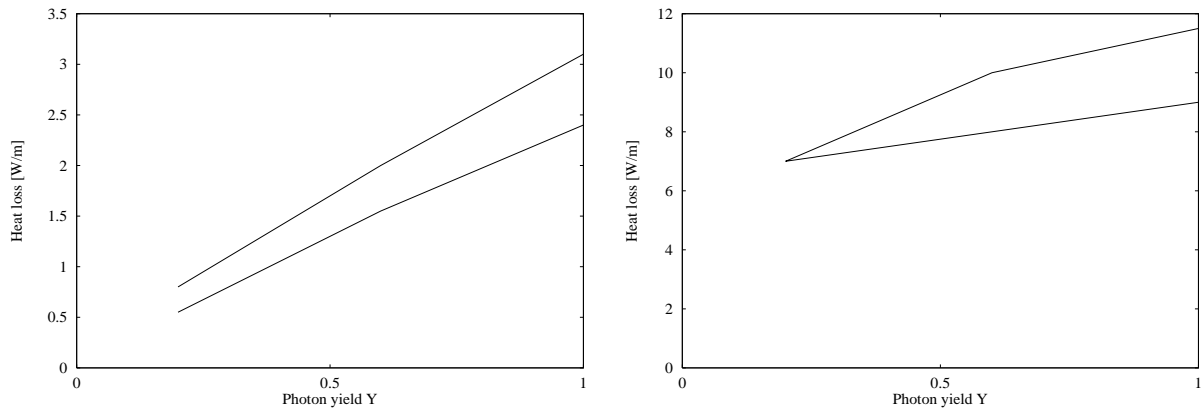


Figure 9: *The heat load in the LHC-type chamber. The top curves correspond to a Gaussian initial energy distribution of the secondary electrons with $\sigma_{se} = 10$ eV and the lower curves to $\sigma_{se} = 20$ eV. Left: $\delta_{max} = 1.066$. Right: $\delta_{max} = 1.8$.*

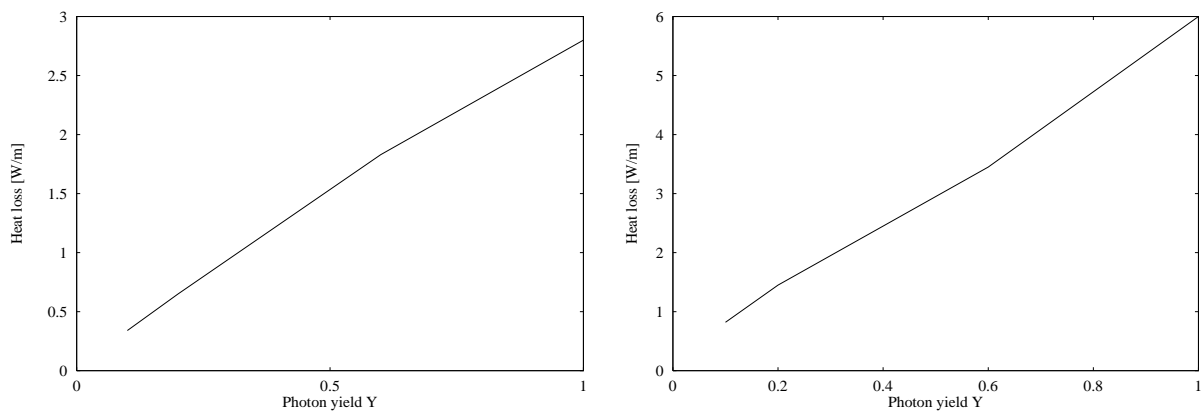


Figure 10: *The heat load in an elliptical chamber for a bunch spacing of 50 ns and $1.48 \cdot 10^{11}$ protons per bunch. Left: $\delta_{max} = 1.066$. Right: $\delta_{max} = 1.8$.*

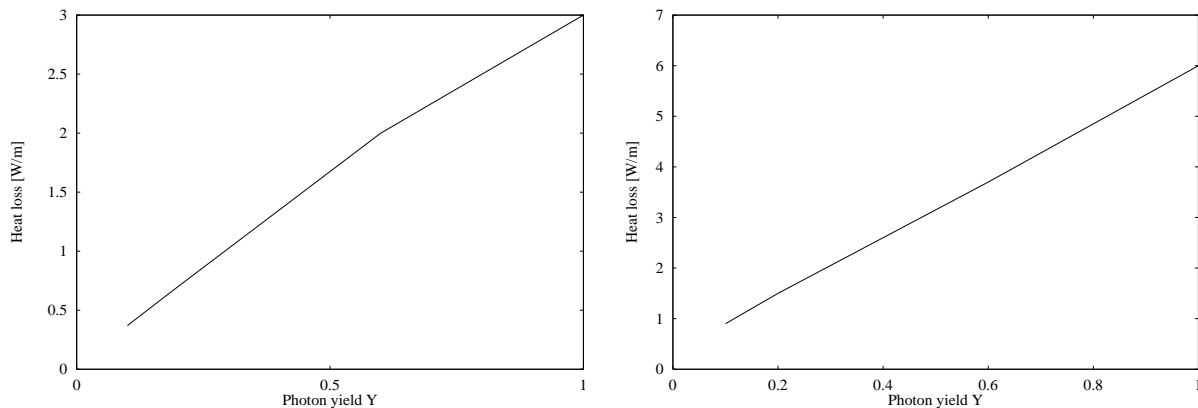


Figure 11: *The heat load in the LHC-type chamber for a bunch spacing of 50 ns and $1.48 \cdot 10^{11}$ protons per bunch. In both cases we assumed a Gaussian initial energy distribution of the secondary electrons with $\sigma_{se} = 10$ eV. Left: $\delta_{max} = 1.066$. Right: $\delta_{max} = 1.8$.*

4.3 Large bunch spacing and bunch current and high reflectivity

Fig. 10 and Fig. 11 show again the heat loss for an elliptical and the LHC-type vacuum chamber. But this time with a bunch spacing of 50 ns and a bunch population of $1.48 \cdot 10^{11}$ protons per bunch. This configurations gives still the same luminosity but clearly a smaller heat loss in the beam screen than the nominal LHC beam parameters. Assuming again a photon yield of $Y = 0.2$ we obtain a heat loss of 0.65 W/m for a secondary emission coefficient of $\delta_{max} = 1.066$ and 1.5 W/m for a secondary emission coefficient of $\delta_{max} = 1.8$. Both values are still larger than the value tolerable by the vacuum system but the heat loss for $\delta_{max} = 1.8$ is clearly smaller than the value for the nominal beam parameters.

4.4 Nominal beam parameters and low reflectivity

In order to account for a small reflectivity, we generate 90% of the synchrotron light photons with a Gaussian angular distribution with $\sigma_\phi = 22.5^\circ$ at one side of the vacuum chamber. 10% of the photo-electrons are still uniformly distributed in the transverse plane. The left-hand side of Figure 12 shows the opening angle of the photo-electrons in the LHC-type vacuum chamber and the right-hand side shows the angular distribution of the photo-electrons around the horizontal plane.

Fig. 13 shows the corresponding heat loss for an elliptical vacuum chamber. The left-hand side of Fig. 13 shows the heat load for a secondary emission yield of $\delta_{max} = 1.066$ and a Gaussian initial energy distribution of the secondary electrons with $\sigma_{se} = 10$ eV. The right-hand side shows the heat load for a secondary emission yield of $\delta_{max} = 1.8$. The lower curves show the heat load versus the photon yield for the new photo electron distribution. For comparison, the top curves show again the heat loss for a high reflectivity.

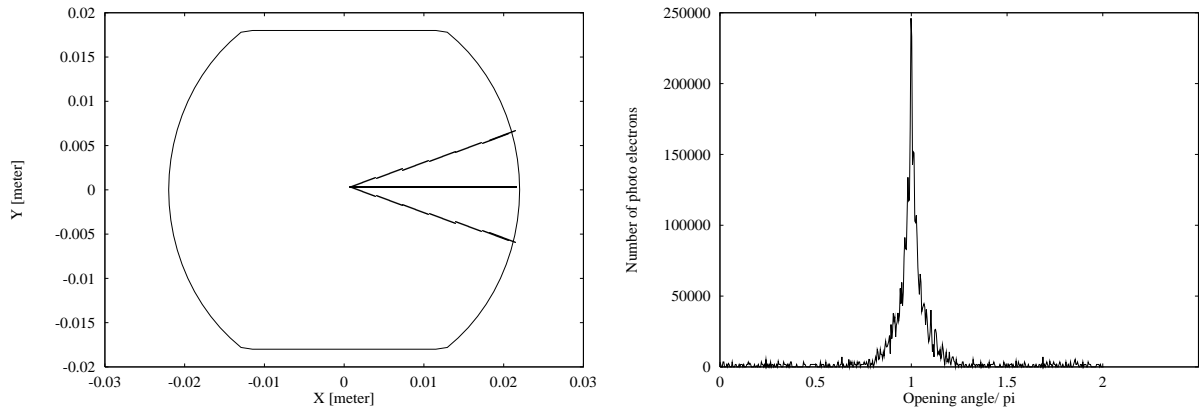


Figure 12:
Left: the opening angle of the photo-electrons in the LHC-type vacuum chamber.
Right: 90% of the photo-electrons are generated with a Gaussian distribution around the horizontal plane with $\sigma_\phi = 22.5^\circ$ and 10% are uniformly distributed in the transverse plane.

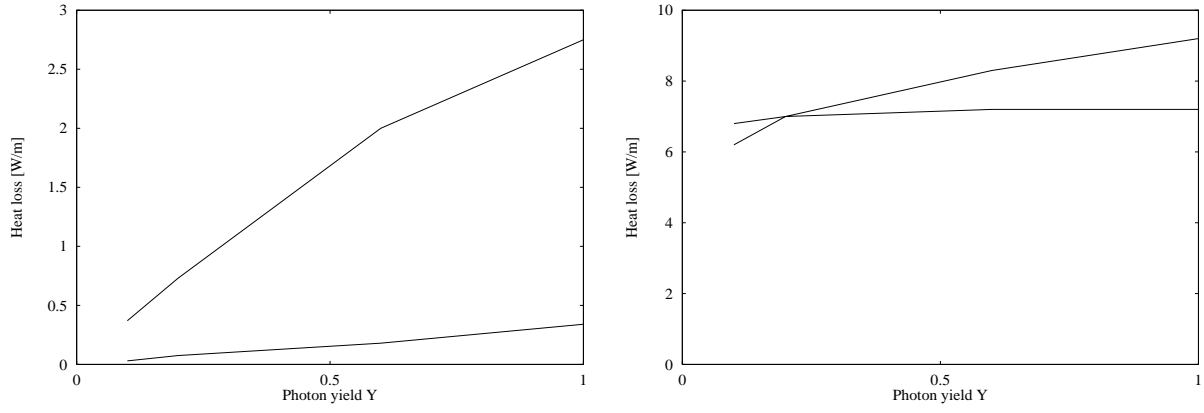


Figure 13: *The heat load in an elliptical chamber for nominal beam parameters. The upper curves show again the heat load versus the photon yield for a uniform distribution of the photo-electrons in the transverse plane. The lower curves show the heat load versus the photon yield for the case where 90% of the photo-electrons are generated with a Gaussian distribution around the horizontal plane with $\sigma_\phi = 22.5^\circ$. 10% are uniformly distributed in the transverse plane.*
Left: $\delta_{max} = 1.066$. Right: $\delta_{max} = 1.8$.

Assuming again a photon yield of $Y = 0.2$ we obtain now a heat loss of $0.08 W/m$ for $\delta_{max} = 1.066$ but still obtain a heat load of $7 W/m$ for $\delta_{max} = 1.8$. As we mentioned earlier, a secondary emission coefficient of $\delta_{max} = 1.8$ is larger than the critical value of $SEY_{crit} = 1.4$ for the nominal beam parameters. In this case, the heat load is mainly determined by the secondary yield and even a small number of photo-electrons is sufficient to trigger the build up of an electron cloud. Thus, the 10% of the photo-electrons which are uniformly generated in the transverse plane give the same heat load as in the case of a high reflectivity. The only difference is that it takes now approximately 20 bunch passages until the electron cloud density reaches its space charge limit compared with approximately 10 bunch passages for the case of a high reflectivity. If we suppress the 10% back-ground of uniformly distributed photo-electrons in the transverse plane, the heat load becomes smaller than $0.1 W/m$ in both cases. However, this scenario requires the absorption of all photo-electrons outside the Gaussian distribution in Fig. 12.

4.5 Large bunch spacing and bunch current and low reflectivity

In this section we assume a bunch spacing of $b_s = 50 ns$ and a bunch intensity of $N_b = 1.48 \cdot 10^{11}$ particles per bunch. We account again for a small reflectivity by generating 90% of the photo-electrons with a Gaussian distribution with $\sigma_\phi = 22.5^\circ$ at one side of the vacuum chamber. Fig. 14 shows the corresponding heat loss for an elliptical vacuum chamber. The left-hand side of Fig. 14 shows the heat load for a secondary emission yield of $\delta_{max} = 1.066$ and a Gaussian initial energy distribution of the secondary electrons with $\sigma_{se} = 10 eV$. The right-hand side shows the heat load for a secondary emission yield of $\delta_{max} = 1.8$. The lower curves show the heat load versus the photon yield for the new photo electron distribution. For comparison, the top curves show again the heat loss for a high reflectivity.

Assuming again a photon yield of $Y = 0.2$ we obtain now a heat loss of $0.074 W/m$ for $\delta_{max} = 1.066$ and $0.14 W/m$ for $\delta_{max} = 1.8$. Both values are now smaller than the limit imposed by the vacuum system. As we mentioned earlier, $SEY_{crit} = 1.4$ increases with increasing bunch spacing. For a bunch spacing of $b_s = 50 ns$ we have $SEY_{crit} = 2.6$ and both secondary emission yields in Fig. 14 are smaller than this value.

4.6 Nominal beam parameters, high reflectivity, and small values of σ_{se}

In the above discussion, we emphasised the effect of the initial energy distribution of the secondary electrons on the critical value δ_{max} . The analysis in Section 3 suggested a particularly high heat load for small values of σ_{se} . However, electrons with small energies are also more easily affected by external forces than electrons with higher energies. For example, very small magnetic fields from the vacuum pumps can affect the measurement of the energy distribution at low energies [5]. In the same way, low energetic secondary electrons will be affected by their own space charge field. In [10] it was suggested that the importance of space charge forces can be estimated by the Debye radius of the electron cloud [11]

$$\lambda_D = 740 \cdot \sqrt{\frac{\bar{E}}{n_e}}; \quad [cm] \quad (11)$$

where \bar{E} is the average kinetic energy in the cloud in eV and n_e the electron density in cm^{-3} . Equating Equation (11) to the pipe radius r_p one can estimate the maximum electron energy

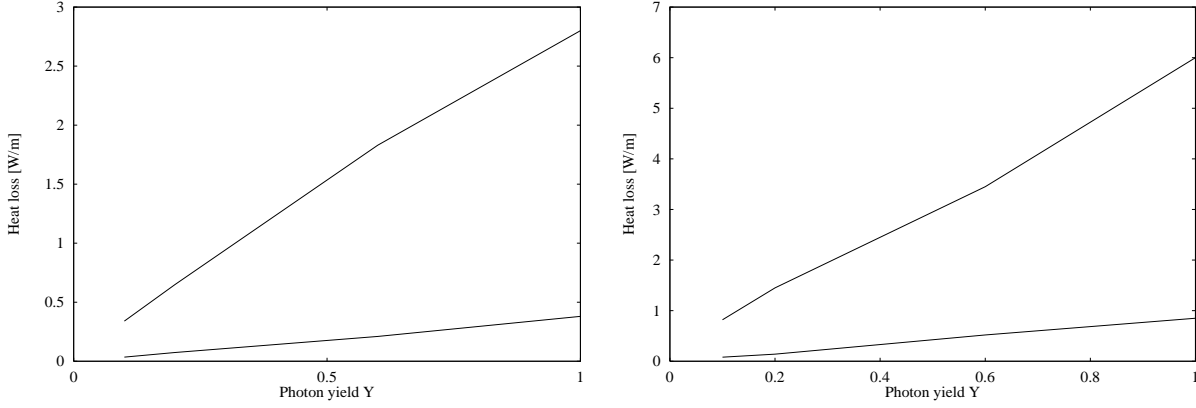


Figure 14: *The heat load in the LHC-type chamber for a bunch spacing of 50 ns and $1.48 \cdot 10^{11}$ protons per bunch. In all cases we assumed a Gaussian initial energy distribution of the secondary electrons with $\sigma_{se} = 10$ eV. The upper curves show again the heat load versus the photon yield for a uniform distribution of the photo-electrons in the transverse plane. The lower curves show the heat load versus the photon yield for the case where 90% of the photo-electrons are generated with a Gaussian distribution around the horizontal plane with $\sigma_\phi = 22.5^\circ$. 10% are uniformly distributed in the transverse plane.*

Left: $\delta_{max} = 1.066$. Right: $\delta_{max} = 1.8$.

for a given density for which the space charge force will be relevant

$$\bar{E} = \frac{r_p^2 \cdot n_e}{740^2}. \quad (12)$$

Assuming a photo yield of $Y = 0.2$ and the nominal LHC beam parameters ($N_p = 1.05 \cdot 10^{11}$) one expects approximately $3.5 \cdot 10^9$ photo-electrons per bending magnet and bunch (Equation (4)). The average energy of the photo-electrons after the bunch passage is 80 eV, leading to an average secondary emission yield of $\langle \delta \rangle \approx 0.5$ at normal incident. Thus, one expects approximately $n_e = 1.2 \cdot 10^5 \text{ cm}^{-3}$ secondary electrons per bending magnet and bunch. Substituting this density of secondary electrons into Equation(12) and taking $r_p = 1.8$ cm, the space charge fields are relevant for electron energies

$$\bar{E} < 1 \text{ eV}. \quad (13)$$

In order to look at this effect in the simulations, we estimate the heat loss in the beam screen as a function of σ_{se} for three different values of δ_{max} :

- $\delta_{max} = 1.066 \rightarrow \delta_{max} < SEY_{crit}$. for all values of σ_{se} .
- $\delta_{max} = 1.8 \rightarrow \delta_{max} > SEY_{crit}$. for all values of σ_{se} .
- $\delta_{max} = 1.2 \rightarrow \delta_{max} = SEY_{crit}$. for $\sigma_{se} = 5$ eV.

Fig. 15 shows the corresponding results for all three cases. For each value of δ_{max} we used two different modes for the space charge calculation. In one case we calculate the space charge field only once, right after the bunch passage and use the resulting space charge field for all intermediate steps in the bunch gap. This method allows a relatively fast simulation but does

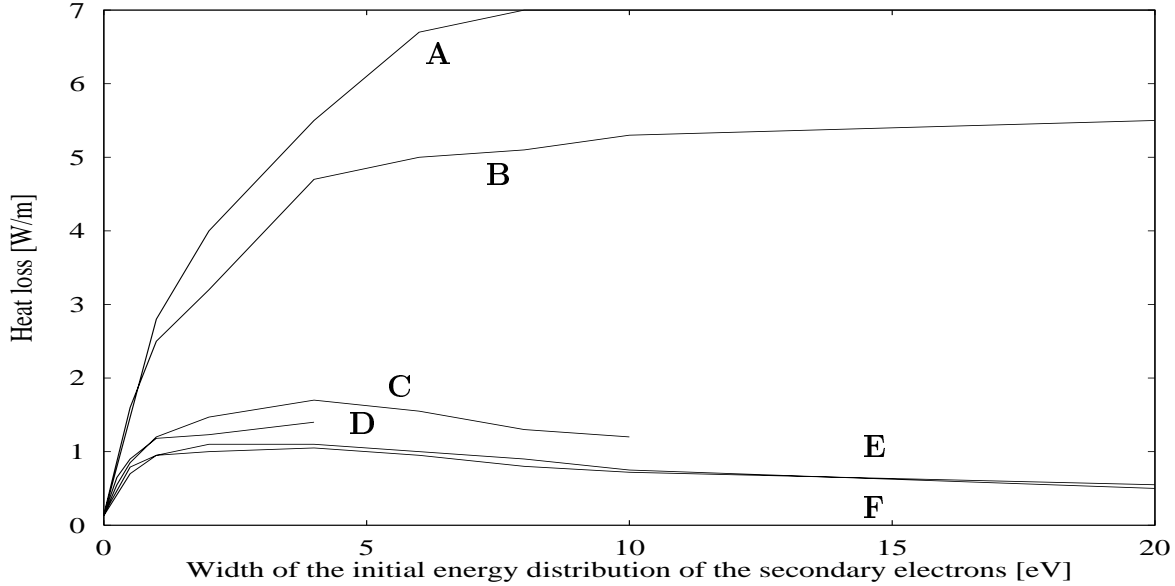


Figure 15: *The heat load in an elliptical chamber versus the width of the initial energy distribution of the secondary electrons for $Y = 0.2$. We assume a Gaussian distribution in all cases and the horizontal axis shows σ_{se} .*

A: $\delta_{max} = 1.8$, the space charge field is calculated only once after the bunch passage.

B: $\delta_{max} = 1.8$, the space charge field is recalculated 10 times after the bunch passage.

C: $\delta_{max} = 1.2$, the space charge field is calculated only once after the bunch passage.

D: $\delta_{max} = 1.2$, the space charge field is recalculated 10 times after the bunch passage.

E: $\delta_{max} = 1.066$, the space charge field is calculated only once after the bunch passage.

F: $\delta_{max} = 1.066$, the space charge field is recalculated 10 times after the bunch passage.

not change the space charge field when the photo-electrons generate new secondary electrons. In the second case, we recalculate the space charge field 10 times in the bunch gap. This method better models the change of the space charge field as new secondary electrons are generated but is very CPU-time consuming. For $\delta_{max} < SEY_{crit}$, the two methods give roughly the same results. This agrees with the intuitive interpretation, that for $\delta_{max} < SEY_{crit}$, the heat load is mainly determined by the photon yield. For $\delta_{max} > SEY_{crit}$, the second method yields a heat load which is up to 30% smaller than the heat loss in the first method. In other words, calculating the space charge field only once right after the bunch passage overestimates the heat load in the beam screen.

In all cases the heat load decreases with decreasing σ_{se} and approaches the value given in Section 4.1 for $\sigma_{se} = 0$. For $\delta_{max} > SEY_{crit}$, the space charge forces start repelling the electrons into the wall of the vacuum chamber for $\sigma_{se} < 7$ eV. In this case, the density of electrons in the cloud is larger than assumed in Equation (12). The left-hand side of Fig.16 shows the evolution of the electron cloud versus time and the right-hand side of Fig. 16 shows the final electron

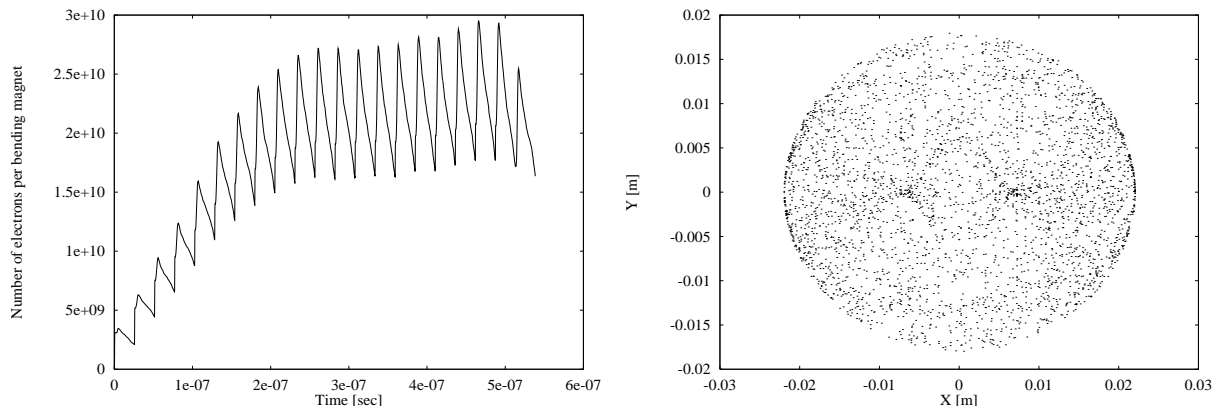


Figure 16: *The electron cloud for $\delta_{max} = 1.8$, $\sigma_{se} = 6$ eV and an elliptical vacuum chamber. Left: The number of electrons per bending magnet versus time. Right: The final electron distribution in the cloud at the end of the bunch gap (after 20 bunch passages).*

distribution at the end of the bunch gap for $\delta_{max} = 1.8$ and $\sigma_{se} = 6$ eV. The data in Fig. 16 gives an average equilibrium electron density of

$$15.6 \cdot 10^5 \text{ cm}^{-3}. \quad (14)$$

Inserting this value into Equation (12) one obtains for the maximum electron energy for which the space charge fields are important

$$\bar{E} \approx 10 \text{ eV}, \quad (15)$$

which is consistent with the results in Fig. 15. For $\delta_{max} < SEY_{crit}$, the space charge forces start repelling the electrons into the wall of the vacuum chamber for $\sigma_{se} < 1$ eV which agrees with the estimate in Equation (13).

5 Potential cures and improvements

In this section, we will briefly discuss four different possibilities for lowering the heat load in the beam screen.

5.1 Lowering the bunch current

The total number of photo-electrons generated per bunch varies linearly and the energy gain of the secondary electrons during the bunch passage quadratically with the number of particles per bunch. The number of photo-electrons per bunch is given in Equation (4) and the energy gain of the secondary electrons during during a bunch passage in the kick-approximation is given by

$$\Delta E = \frac{(\Delta p)^2}{2 \cdot m_e}; \quad \Delta p \approx \frac{2N_b r_e c m_e}{r}, \quad (16)$$

where r_e is the classical electron radius, m_e the electron rest mass and r the distance of the electron to the bunch. Thus, one would expect a cubic dependence of the heat load on the

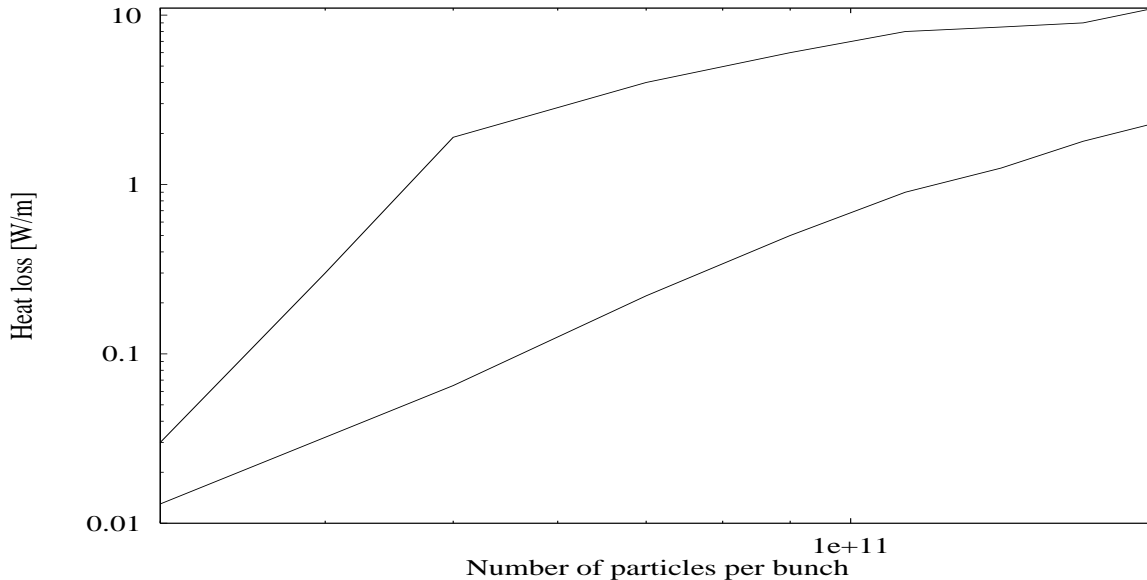


Figure 17: *The heat load in an elliptical chamber versus the bunch intensity on a double logarithmic scale. The top curve shows data for $\delta_{max} = 1.8$ and the lower curve for $\delta_{max} = 1.066$. In both cases we assumed $Y = 0.2$ and $\sigma_{se} = 10$ eV.*

bunch intensity. Furthermore, if the average energy gain of the photo-electrons is lower than the critical energy E_{max} where the secondary emission yield has a maximum, the secondary emission yield also changes approximately linearly with the bunch intensity. Fig. 3 showed that the average energy gain of the photo-electrons is approximately 80 eV for the nominal LHC beam parameters. In all simulations we assume $E_{max} = 400$ eV and we expect the heat load to change with the fourth power of the bunch current for bunch intensities smaller than the nominal value of $N_b = 1.05 \cdot 10^{11}$. Fig. 17 shows the heat loss versus the bunch intensity on a double logarithmic scale. The top curve shows data for $\delta_{max} = 1.8$ and the lower curve for $\delta_{max} = 1.066$. In both cases we assumed $Y = 0.2$ and $\sigma_{se} = 10$ eV. For $\delta_{max} < SEY_{crit}$, the heat load is mainly determined by the photo-electrons and the contribution of the secondary electrons has no strong effect. Thus, one would expect a cubic dependence of the heat load on the bunch intensity in this case. The data for $\delta_{max} = 1.066$ agrees nicely with this prediction. The lower curve in Fig. 17 for $\delta_{max} = 1.066$ has an average slope of 2.98. For $\delta_{max} > SEY_{crit}$, one expects a large contribution of the secondary electrons on the heat load and the heat load should vary with the fourth power of the bunch intensity for high bunch intensities and only with the third power for small bunch intensities. Again, the data in Fig. 17 agrees nicely with this estimate. The slope of the upper curve in Fig. 17 for $\delta_{max} = 1.8$ has a slope of 4.0 for bunch intensities smaller than $N_b = 0.5 \cdot 10^{11}$ and an average slope of 2.8 for bunch intensities larger than $N_b = 0.5 \cdot 10^{11}$.

Assuming $\delta_{max} = 1.8$, $Y = 0.2$ and $\sigma_{se} = 10 \text{ eV}$ one has to limit the bunch intensity to

$$N_b = 0.4 \cdot 10^{11} \quad (17)$$

particles per bunch for a heat loss of less than 0.2 W/m . For smaller values of σ_{se} the required reduction of the bunch current should be smaller (see Fig. 15). The discussion in Section 4.3 showed that one can further improve the heat loss by increasing the bunch spacing in the LHC. Taking a bunch spacing of 50 ns and a bunch population of $1.48 \cdot 10^{11}$ protons per bunch and $Y = 0.2$ we obtained a heat load of 1.5 W/m for a secondary emission coefficient of $\delta_{max} = 1.8$. Assuming a cubic scaling of the heat loss with the bunch intensity, one has to reduce the bunch intensity by a factor 1.95 in order to keep the heat loss below 0.2 W/m . In this case, the total luminosity would be reduced by almost a factor of four, part of which could potentially be recovered by a smaller emittance (the reduced intensity of $N_b = 0.76 \cdot 10^{11}$ protons per bunch is smaller than the nominal design value).

5.2 Synchrotron light absorption

The discussion in Sections 4.4 and 4.5 showed that the heat loss in the dipole magnets can be significantly reduced by generating the photo-electrons only on one side of the vacuum chamber in the horizontal plane. Because of the strong vertical magnetic field in the dipoles, the electrons are bound to a motion along the vertical field lines and electrons generated at the vacuum chamber near the horizontal plane can never reach the center of the vacuum chamber. Thus, the energy gain for these electrons is proportional to $\sin \alpha$, where α is the angle of the position of the electron with respect to the horizontal plane. Without a strong vertical magnetic field, the spatial distribution of the photo-electrons has no effect on the heat load.

Generating new photo-electrons only on one side of the vacuum chamber in the horizontal plane implies either a very low surface reflectivity or the utilisation of synchrotron light absorbers. Fig. 18 shows the heat load as a function of the opening angle in which the photo-electrons are generated (see Fig. 12). In both cases we assumed $Y = 0.4$, $\delta_{max} = 1.5$ and $\sigma_{se} = 10 \text{ eV}$. The space charge field was recalculated 10 times during the bunch gap. For the left-hand side of Fig. 18 we generated 90% of the photo-electrons with a Gaussian angle distribution at one side of the vacuum chamber. 10% of the photo-electrons are still uniformly distributed in the transverse plane. For the right-hand side of Fig. 18 we generated all photo-electrons with a Gaussian angle distribution with at one side of the vacuum chamber. Generating only 90% of all photo-electrons with a Gaussian distribution with $\sigma_\phi < 50^\circ$ at one side of the vacuum chamber is already sufficient for reducing the heat load to less than 0.2 W/m . For a uniform distribution of the photo-electrons in the transverse plane we get a heat load of 1.7 W/m . Generating all photo-electrons with a Gaussian distribution with $\sigma_\phi < 50^\circ$ at one side of the vacuum chamber reduces the heat loss to less than 0.02 W/m . Therefore, obtaining a reliable estimate for the opening angle of the photo-electrons in the LHC beam screen would provide an important input parameter for the heat load estimate. So far, most estimates assumed a worst case scenario where the photo-electrons are uniformly generated in the transverse plane of the vacuum chamber.

5.3 Solenoid field

One proposal for avoiding the build up of an electron cloud is to generate a weak solenoid field which bends newly generated secondary electron back to the wall of the vacuum chamber.

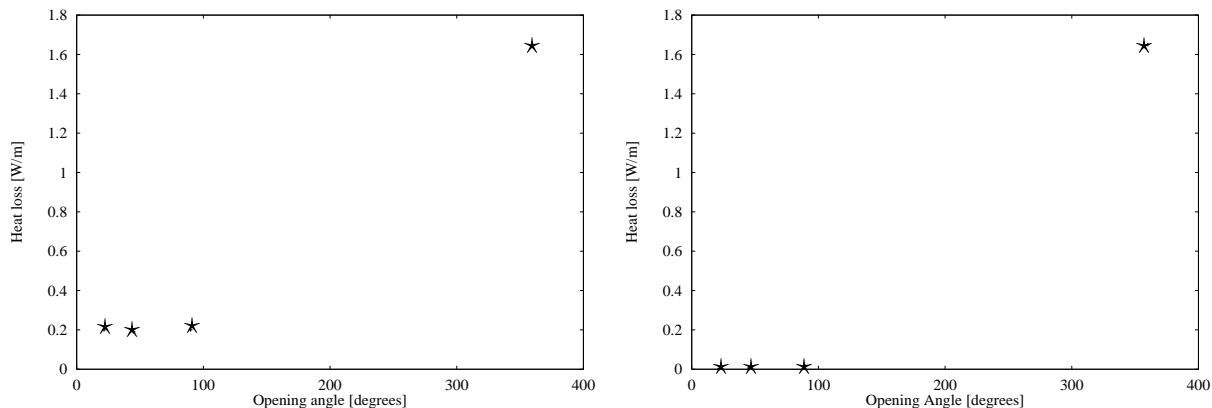


Figure 18: *The heat load as a function of the opening angle σ_ϕ in which the photo-electrons are generated.*

Left: 90% of the photo-electrons are generated with a Gaussian distribution at one side of the vacuum chamber. 10% of the photo-electrons are still uniformly distributed in the transverse plane.

Right: All photo-electrons are generated with a Gaussian distribution at one side of the vacuum chamber.

For example, in the KEK B-factory it is foreseen to use a solenoid field between 10 G and 20 G [1]. A similar setup could be a solution for the field free regions in the LHC, where first simulation results indicate a heat load which is a factor three larger than in the dipole magnets [13]. For example, we mentioned in Section 3 that the experimental insertion might have a particularly high heat loss. With a solenoid field on, this will not be true. However, one has to keep in mind that it might be desirable to operate the machine with the strong experimental solenoid fields turned off. In this case it would be desirable to have an additional weak solenoid field which can be turned on independently from the solenoids in the experiments. However, a solution with solenoids would probably be ineffective in the dipole magnets where any electron motion will be dominated by the strong vertical field of 8.4 T . This issue is investigated at the moment.

5.4 Secondary emission yield

Fig. 19 shows the heat loss in an elliptical chamber versus the secondary emission yield parameter δ_{max} . The other parameters are $N_b = 1.05 \cdot 10^{11}$ particles per bunch, $b_s = 25$ ns, $\sigma_{se} = 10$ eV and $Y = 0.2$. All photo-electrons are generated uniformly in the transverse plane. The heat load varies from approximately 0.5 W/m for $\delta_{max} \approx 1.0$ to more than 15 W/m for $\delta_{max} > 2.5$ illustrating again the need to carefully select a surface material with a secondary emission yield as low as possible. However, even a TiN coating with $\delta_{max} = 1.066$ yields already a heat load of more than 0.5 W/m with the above parameters and assumptions and it is essential also to limit the photon yield and reflectivity of the beam screen surface.

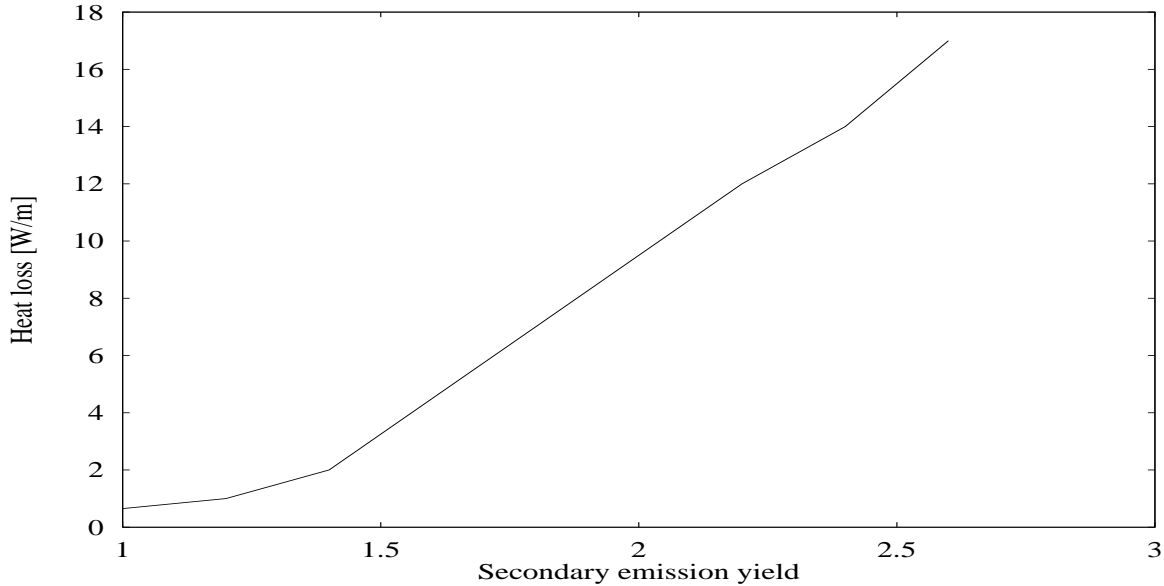


Figure 19: *The heat load in an elliptical chamber versus the secondary emission yield δ_{max} . In all cases we assumed $N_b = 1.05 \cdot 10^{11}$ particles per bunch, $b_s = 25$ ns, $\sigma_{se} = 10$ eV and $Y = 0.2$.*

5.5 Vertical electrostatic field

Even a weak vertical electrostatic field can significantly reduce the heat load in the dipoles by pulling the low energetic secondary electrons back into the vacuum chamber [4]. However, cutting the beam pipe in two electrically isolated parts and applying a DC-voltage between the two parts is difficult to realise and implies other problems for the transverse impedance. An alternative method could be to use stretched wires at the corners of the beam screen. The left-hand side of Fig. 20 shows the position of the wires used in the simulations and the right-hand side shows the corresponding electric field lines in an elliptical vacuum chamber for a negative DC-bias of the wires. A first analysis of such a solution for secondary electrons with a Gaussian initial energy distribution with $\sigma_{se} = 5$ eV shows that one can reduce the heat loss in the dipole magnets by more than one order of magnitude. The efficiency of this solution should increase with decreasing values of σ_{se} and more simulations and experiments are required for realistically judging the effect of this method. Fig. 21 shows the heat loss in the beam screen as a function of different voltages between the wires and the beam screen surface. In all cases we assumed nominal LHC beam parameters with $N_b = 1.05 \cdot 10^{11}$ particles per bunch and a bunch separation of $b_s = 25$ ns, a photon yield of $Y = 0.2$ and a secondary emission yield coefficient of $\delta_{max} = 1.8$. A voltage of only 20 Volt decreases the heat loss in the beam screen from approximately 6 W/m to less than 0.2 W/m. However, it is not clear if such a solution could be realised from the hardware and aperture point of view. Nevertheless, it illustrates how the low energetic secondary electrons are influenced even by very small external perturbations.

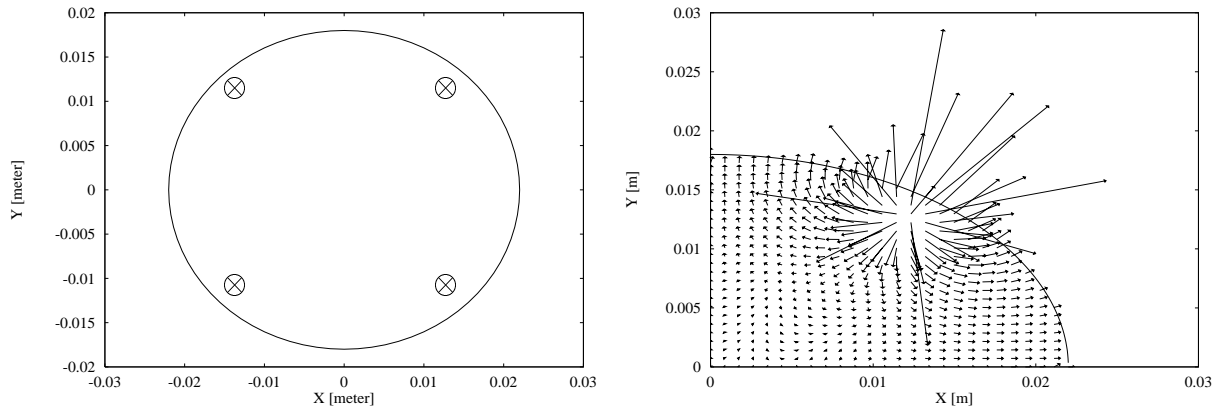


Figure 20:

Left: Stretched wires inside the vacuum chamber.

Right: The corresponding electric field lines in an elliptical vacuum chamber.

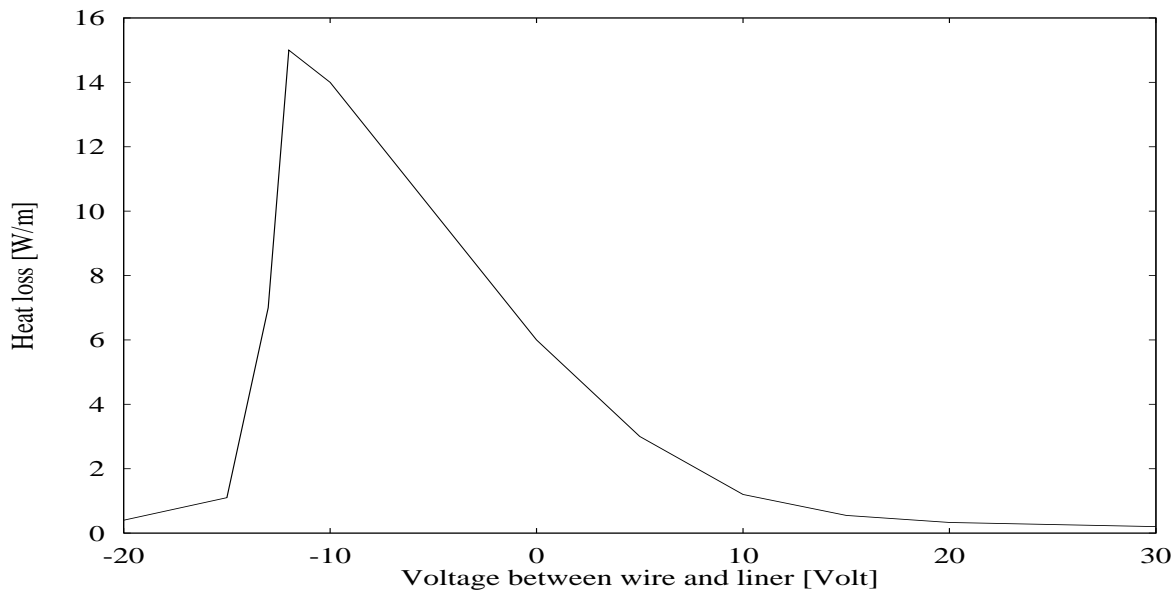


Figure 21: *The heat loss in an elliptical chamber versus the voltage between a stretched wire in the chamber and the chamber wall. In all cases we assumed $N_b = 1.05 \cdot 10^{11}$ particles per bunch, $b_s = 25$ ns, $\sigma_{se} = 10$ eV, $Y = 0.2$ and $\delta_{max} = 1.8$.*

6 Summary

The numerical simulations for the beam induced electron cloud show that the resulting heat loss in the dipole magnets can vary between $0.01 W/m$ and more than $15 W/m$ depending on the input parameters. The most important surface parameters are the photon yield Y , the secondary emission coefficient δ_{max} , the initial energy distribution of the secondary electrons and the surface reflectivity R for the beam screen inside the dipole magnets. The photon yield has been recently measured at CERN for different Cu surfaces and we assume $Y = 0.2$ for most of our estimates. Another important parameter is the secondary emission coefficient δ_{max} which determines how many secondary electrons are generated per incident electron. If the secondary emission coefficient of the vacuum chamber is smaller than a critical value $SEY_{crit.}$, the heat loss will be proportional to the synchrotron light illumination and the photon yield. If it is larger than this value, the heat loss will be determined by the value of δ_{max} and even a small number of initial electrons is sufficient to trigger the build up of an electron cloud. The value of $SEY_{crit.}$ depends on the beam parameters, the energy distribution of the secondary electrons and the vacuum geometry. Clearly, when designing a beam screen for the LHC vacuum chamber it is important to achieve a secondary emission coefficient which is smaller than the critical yield value. For the nominal LHC parameters and secondary electrons with a Gaussian distribution for the initial energy with $\sigma_{se} = 10 eV$, the critical secondary emission yield is $SEY_{crit} \approx 1.4$. By doubling the bunch spacing in the LHC and increasing the bunch intensity in order to keep the luminosity constant, the value of SEY_{crit} can be increased to $SEY_{crit} > 2.5$. The secondary emission coefficient of most materials available for the LHC beam screen is larger than $\delta_{max} = 1.8$.

The value of SEY_{crit} decreases with σ_{se} making it difficult, if not impossible, to find a surface material with $\delta_{max} < SEY_{crit}$ for low energetic secondary electrons. Fortunately, for distribution widths with $\sigma_{se} < 5 eV$ the secondary electrons are affected by their own space charge field and newly generated electrons are repelled into the vacuum chamber. In this case, the heat loss decreases with decreasing σ_{se} for all values of δ_{max} and it is not anymore important that the secondary emission coefficient of the surface material is smaller than the critical secondary emission yield SEY_{crit} .

Thus an accurate estimate of the heat loss depends on an accurate measurement of the distribution function of the initial energy of the secondary electrons. First measurements of the distribution of the initial energy of the secondary electrons indicate a distribution with mostly low energetic electrons. Unfortunately, the measurement of low energetic electrons is rather difficult and an accurate estimate for the distribution function is not yet available. The difficulty of measuring the distribution function of low energetic electrons illustrates how easily these electrons are influenced by an external field and indicates several possibilities for eliminating the newly generated secondary electrons. For example, small solenoid or electrostatic fields can deflect or redirect the secondary electrons in the LHC beam screen back to the beam pipe before the next bunch arrives.

The reflectivity of the surface material in the beam screen is another important input parameter for estimating the heat loss. However, while it is rather straightforward to measure the reflectivity for a given surface and synchrotron light spectrum, it is rather difficult to estimate how this reflectivity affects the initial spatial distribution of the photo-electrons in the vacuum chamber. For example, the final spatial distribution of the photo-electrons depends also on the orbit of the proton beam. Again, we can only estimate the resulting heat loss for different

spatial distributions without knowing what the real distribution in the LHC beam screen looks like. Assuming a photon yield of $Y = 0.2$ and a secondary emission yield of $\delta_{max} = 1.8$, the most pessimistic estimates for the heat load yield $5 W/m$ for a uniform distribution of the photo-electrons in the transverse plane (100% reflectivity). Doubling the bunch spacing in the machine with a bunch intensity of $N_b = 1.48 \cdot 10^{11}$ particles per bunch and generating only 90% of the photo-electrons with a Gaussian distribution with $\sigma_\phi = 22.5^\circ$ at one side of the vacuum chamber while distributing 10% of the photo-electrons uniformly in the transverse plane yields a heat load of $0.14 W/m$. Generating all photo-electrons with a Gaussian distribution with $\sigma_\phi = 22.5^\circ$ at one side of the vacuum chamber yields a heat load of less than $0.02 W/m$. Thus, the final result depends on the spatial distribution of the photo-electrons in the vacuum chamber and estimating/measuring this distribution is a key requirement for an accurate analysis. Another possibility would be to generate the desired spatial distribution of photo-electrons by introducing synchrotron light absorbers into the beam screen.

By allowing the option of doubling the bunch distance in the machine, a worst case scenario with 100% reflectivity, $\sigma_{se} = 10 eV$ and $\delta_{max} = 1.8$ would limit the number of particles per bunch to $N_b = 0.76 \cdot 10^{11}$ compared with a nominal design intensity of $N_b = 1.05 \cdot 10^{11}$. In this case the total luminosity would be reduced by a factor four, part of which could be recovered by a smaller emittance of the beam. For smaller values of σ_{se} or smaller reflectivities, the reduction in bunch intensity is lower.

The main goal of the presented study was to provide upper estimates for the heat loss in the beam screen and to analyse the dependence of the heat loss on different parameters. The presented results underline the importance of accurately measuring the spatial distribution of the photo-electrons in the vacuum chamber for a given surface reflectivity and the initial energy distribution of the secondary electrons.

Acknowledgements

I would like to thank Francesco Ruggiero for initiating this study and for numerous stimulating discussions. Ian Collins and Oswald Gröbner are acknowledged for providing a good feed back from the measurements at the EPA ring. I thank Miguel Furman for his collaboration and for sharing his simulation results. I thank Gennady Stupakov for many interesting discussions during his stay at CERN. I also want to thank Michael Böge and Frank Schmidt for their support on the NAP computer. Without a powerful computer system a study like this would not have been possible.

References

- [1] S. Hiramatsu, 'Solenoid design for sweeping photo electrons at KEKB', proceedings of the International workshop on multibunch instabilities in future electron and positron accelerators', Tsukuba, July 1997.
- [2] M. Furmann, LHC Project Report in preparation.
- [3] F. Zimmermann 'A Simulation Study of Electron-Cloud instability and Beam-Induced Multipactoring in the LHC' LHC Project Report 95 (1997).
- [4] O. Brüning, 'Simulations for the Beam-induced Electron Cloud in the LHC liner', LHC Project Note 102, 1997.
- [5] I. Collins and O. Gröbner, private communication, September 1997.
- [6] M. Sands, 'The physics of Electron Storage Rings', SLAC-121 (1970).

- [7] H. Seiler, 'Secondary electron emission in the scanning electron microscope', Phys. **54** (11) (1983).
- [8] J.B. Jeanneret, 'Photoemission in LHC - A simple model', CERN SL/Note 97-48 (AP).
- [9] M. Furman 'The Electron-Cloud Effect for LHC', Proceedings of the international workshop on multibunch instabilities in future electron and positron accelerators, Tsukuba, Japan 1997.
- [10] G. Stupakov 'Photoelectrons and Multipacting in the LHC: Electron Cloud Build-up', LHC Project Report 141, 1997.
- [11] F. Chen, 'Introduction to Plasma Physics', Plenum Press, New York and London, 1976.
- [12] J. Barnard, Y. Bozko, G. Dominichini, N. Hilleret and J.M. Jimenez, Proceedings of the seventh workshop on RF superconductivity, Gif sur Yvette, France, 1995
- [13] M. Furmann, private communication, November 1997.